



DOI: [10.29026/oes.2024.230020](https://doi.org/10.29026/oes.2024.230020)

Deblurring, artifact-free optical coherence tomography with deconvolution-random phase modulation

Xin Ge¹, Si Chen¹, Kan Lin¹, Guangming Ni⁴, En Bo¹, Lulu Wang¹ and Linbo Liu^{1,2,3*}

¹School of Electrical and Electronic Engineering, Nanyang Technological University, Singapore 639798, Singapore; ²School of Chemical and Biomedical Engineering, Nanyang Technological University, Singapore 637459, Singapore; ³China-Singapore International Joint Research Institute (CSIJRI), Guangzhou 510000, China; ⁴School of Optoelectronic Science and Engineering, University of Electronic Science and Technology of China, Chengdu 610054, China.

*Correspondence: LB Liu, E-mail: liulinbo@ntu.edu.sg

Supplementary information for this paper is available at <https://doi.org/10.29026/oes.2024.230020>



Open Access This article is licensed under a Creative Commons Attribution 4.0 International License.

To view a copy of this license, visit <http://creativecommons.org/licenses/by/4.0/>.

© The Author(s) 2024. Published by Institute of Optics and Electronics, Chinese Academy of Sciences.

In addition, we recorded the B-scans of human labial mucosa *in vivo* using μ -OCT. It can be seen that the Deconv-RPM image (Fig. S1(b)) is much sharper than the conventional OCT image (Fig. S1(a)) and the deconvolved image (Fig. S2) throughout the depths. Specifically, nonkeratinized epithelial cells seen as nucleocytoplasmic boundaries can be unambiguously discerned (Fig. S1(c) and S1(d), pink arrowheads in green dashed-line box). Moreover, inside a blurred, noisy vessel in the deep tissue fine structures (pink arrowheads in orange dashed-line box), presumably red blood cells, can be clearly visualized by Deconv-RPM, illustrating the expected deblurring capability and the reduction of noise. Fig. S1(g) and S1(h) show the volume-rendered epithelium with both the unprocessed and the reconstructed data. 10 frames averaging of the *en-face* images shows the high scattering signals from the nucleocytoplasmic boundaries. In Supplementary Movie S2, the depths relative to the epithelium are presented in the *x-y* views *in vivo*.

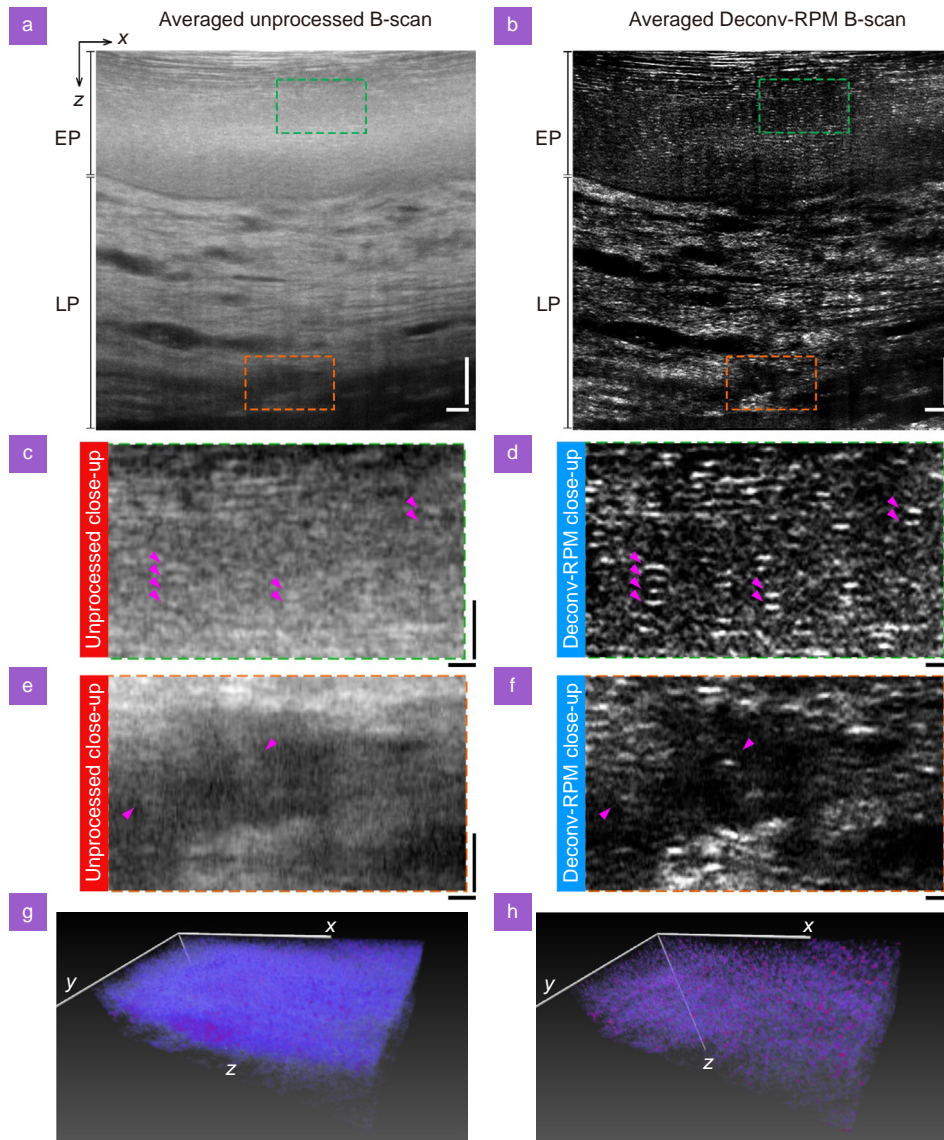


Fig. S1 | *In vivo* imaging of human labial mucosa. (a, b) Conventional μ -OCT and Deconv-RPM imaging of human labial mucosa with 50 B-scan averages. EP: epithelium, LP: lamina propria. Scale bars, 50 μ m. (c, d) Zoomed view on high-scattering nucleocytoplasmic boundaries in the mucosal epithelium. Scale bars, 10 μ m. (e, f) Localized structures in the blood vessel are clearly visible in the magnified image (4 \times). Brightness scaling of each image was set as the respective minimum and maximum to prevent over-saturation. Scale bars, 10 μ m. (g, h) Reconstruction of Deconv-RPM data can be seen to significantly improve image quality over unprocessed OCT data. 10 frames were averaged in the *en-face* plane.

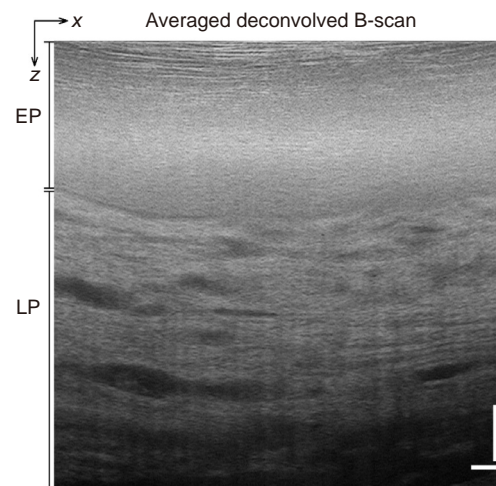


Fig. S2 | Imaging of human labial mucosa with 50 B-scan averages processed by deconvolution only. EP: epithelium, LP: lamina propria. Scale bars, 50 μm .

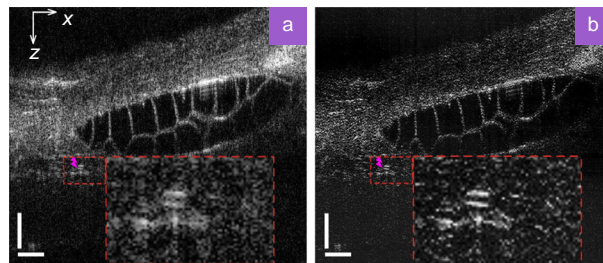


Fig. S3 | *In vivo* imaging of zebra fish larvae. (a) A representative $\mu\text{-OCT}$ showing an individual RBC in the tail artery (highlighted orange box and inset). Scale bars in the main figure: 50 μm . An individual RBC appears as a pair of distinct signals (marked by pink arrows) originating from the top and bottom surfaces of the disk-shaped cell body. (b) This individual RBC is clearly resolved by the Deconv-RPM. The Inset shows a 4 \times magnified view.